communications earth & environment

Article

A Nature Portfolio journal

https://doi.org/10.1038/s43247-025-03030-5

Irrigation cooling effect reduced by water-saving practices

Chao Zhang [1,2], Quansheng Ge [1] ✉, Wim Thiery [3], Yan Li [4], Shushi Peng [5], Guoyong Leng [1], Guosong Zhao [6], Zhenong Jin [7], Wei Li [8], Kun Zhang [9], Xuezhen Zhang [1], Songjun Han [10], Geli Zhang [11], Xiangming Xiao [12] & Jinwei Dong [1] ✉

Irrigation modifies land-atmosphere interactions, cooling land surface and mitigating heat extremes. However, the global shift toward water-saving irrigation technologies raises new questions about the climate regulation capacity of irrigation under constrained water use. Using two decades of high-resolution satellite observations across China, we show that widespread water-saving adoption has substantially weakened irrigation's biophysical cooling effects, particularly in late summer and early spring. Daytime land surface cooling declined by 0.05 K/decade (15%) nationally and up to 0.20 K/decade (9%) in arid regions, primarily due to reduced soil evaporation and increased sensible heat flux. This trend was absent in semi-arid and semi-humid regions because of enhanced crop transpiration. Conversely, nighttime cooling intensified by 0.04 K per decade, likely driven by lower soil thermal capacity and radiative feedbacks. These findings reveal an emerging trade-off between water-use efficiency and climate mitigation, calling for considering evolving irrigation practices in Earth system models and climate change projections.

Climate change is intensifying heat extremes, drought frequency, and water scarcity, posing escalating risks to food production, ecosystem stability, and rural livelihoods[1,2]. As the backbone of global agriculture, irrigation has long served as a primary adaptation strategy to buffer crop growth against these growing drought and heat threats[3,4], especially in arid and semi-arid regions. Beyond its agronomic benefits, irrigation modifies land-atmosphere interactions by modulating surface energy budgets (e.g., increasing latent heat flux)[5]. Numerous observational and modeling studies have documented the irrigation-induced cooling of land surface temperature (LST) and near-surface air temperature, particularly during the daytime[6–11]. Accordingly, irrigation is increasingly viewed not only as an adaptive tool for crop resilience but also as a biophysical mechanism that mitigates local warming[12].

However, this narrative is changing. Across many water-stressed regions of the world, irrigation practices are undergoing a profound transformation. Water-saving irrigation technologies (denoted as WSI hereafter)—such as drip, sprinkler, and precision irrigation—are being promoted as cornerstones of climate-smart agriculture, to maximize crop water productivity while minimizing unsustainable withdrawals[13–15]. In China alone, per-hectare irrigation water use has declined by more than 30% since 2000[16], concurrent with a national campaign to expand WSI technologies[17]. While this transition supports more sustainable water management, it is interesting to know whether the biophysical cooling results from years of inefficient irrigation practices is being preserved—or inadvertently weakened—as irrigation becomes more efficient. The impacts of irrigation on surface water cycle and energy budgets have been reported to depend largely on the choice of irrigation methods (e.g., sprinkler, drip, and flood irrigation)[18–20]. For instance, drip irrigation is found to generate the least surface cooling among the three methods, while recognized as the most water-saving method[20]. Incorporating more realistic irrigation methods in next-generation models is also advised to improve the representation of the hydrological and climatic impacts attributed to anthropogenic land use changes[10].

Nevertheless, most existing Earth system models and climate policy assessments still treat irrigation as a static and spatially homogeneous land surface process[6,21]. This assumption may obscure the evolving climate impacts of irrigation, particularly as WSI adoption accelerates under increasing water scarcity. Recently, studies based on both in-situ climate stations and satellite observations revealed the declining irrigation cooling effect on surface temperature in Northwest China, due to the prosperous WSI promotion[22–24]. However, previous studies have largely focused on arid regions, limiting their generalizability across diverse climate zones. Moreover, the mechanisms driving spatial variations in irrigation-induced cooling remain poorly understood, hindering a comprehensive understanding of irrigation's evolving role in mitigating climate warming. Meanwhile, empirical research has lagged in quantifying how reduced water inputs under WSI affect land surface energy partitioning and temperature regulation at scale[22,23]. In particular, the diurnal asymmetry of these effects—the differential responses of daytime and nighttime LST to irrigation water

A full list of affiliations appears at the end of the paper. ✉e-mail: geqs@igsnrr.ac.cn; dongjw@igsnrr.ac.cn

use changes—remains poorly understood and is largely absent from global climate simulations[25,26]. These diurnal differences carry important implications for crop stress, atmospheric boundary layer development, and energy demand patterns[27]. There is thus an urgent need to integrate observational evidence of WSI-induced land surface changes into both climate assessments and land-atmosphere modeling frameworks.

This study addresses key empirical and modeling gaps by providing the first large-scale observational assessment of how WSI alters irrigation-induced climatic effects. Focusing on China—a region experiencing rapid WSI expansion and high spatial heterogeneity—as a high-resolution natural laboratory, we tested two hypotheses: (1) that widespread WSI implementation has attenuated irrigation's cooling effect, thereby contributing to regional warming; and (2) that the direction and magnitude of these effects vary across space and time, depending on WSI intensity and local climatic conditions. To investigate, here we used the declining irrigation water use (IWU) per unit cropland area[16] as a proxy for the expanding WSI—the shift from traditional flood irrigation to more efficient irrigation practices. Based on an improved long-term irrigation area dataset we produced earlier[28] (Methods), we first extracted the changes in satellite-observed LST from MODIS (difference in LST between irrigated and nearby non-irrigated areas, denoted as ΔLST hereafter) and concurrent changes in energy fluxes caused by irrigation at the 1-km pixel scale. We then quantified their temporal trends at various temporal (annual, seasonal, and diurnal) and spatial (national, climate zone, and provincial) scales. Last, we explored the underlying mechanisms by examining the relationship between temporal trends in ΔLST and irrigation water consumption, as well as the background climatic and environmental factors (Methods). Our findings about the varying irrigation cooling trends across climate zones and the underlying mechanisms due to increasing water-saving practices highlight the importance of considering land management changes in models for projecting future climate changes.

Results

Declining water use and contrasting diurnal land surface cooling trends

The expansion of WSI across China has substantially reduced IWU over the past two decades. Nationally, per-hectare IWU declined by over 30% from 2001 to 2020 (Fig. 1a), with consistent decreases observed across both regional and provincial scales (Fig. 1b–e; Supplementary Fig. 1). This declining trend in irrigation intensity coincided with marked diurnal changes in LST associated with irrigation.

On average, irrigation produced a daytime cooling effect of −0.34 ± 0.04 K across continuously irrigated croplands in China during 2001–2020 (Supplementary Fig. 2; Supplementary Text 1). However, this cooling effect weakened significantly over time, with a national mean trend of 0.05 K (15% relative to the 20-year mean) per decade ($p < 0.05$; Fig. 1e),

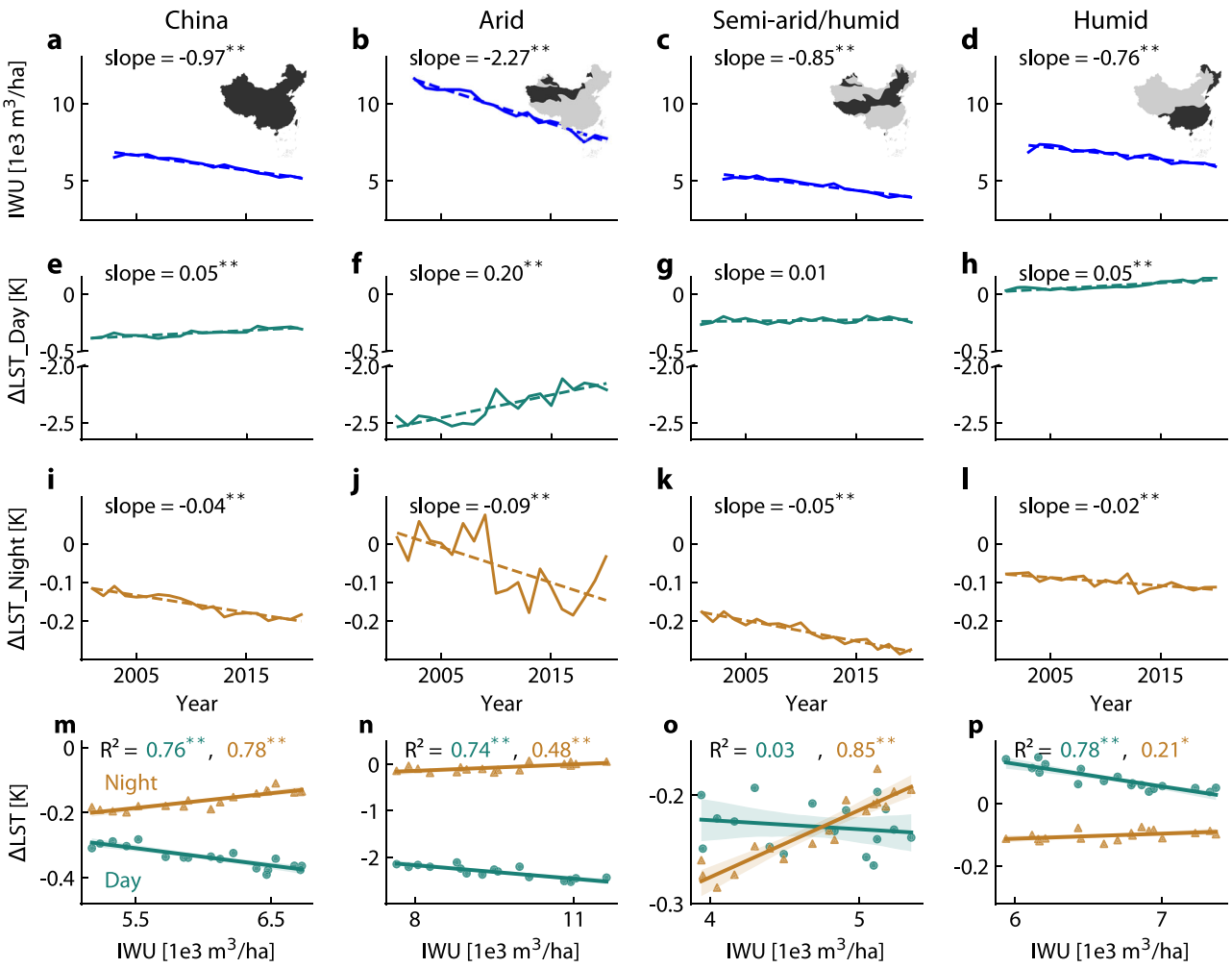

Fig. 1 | Trends in irrigation water use (IWU) and irrigation-induced land surface temperature change (ΔLST) from 2001 to 2020. a–d Temporal trends in IWU across China and different climate zones over the last two decades (unit: 10^3 m^3/ha/decade). **e–h** Temporal trends in daytime ΔLST (unit: K/decade). **i–l** Temporal trends in nighttime ΔLST (unit: K/decade). **m–p** Scatter plots showing the relationship between IWU and ΔLST in China and different climate zones. In all panels, $^{**}p < 0.05$ and $^{*}p < 0.10$ denote statistical significance based on Student's *t*-test. Shaded areas represent 95% confidence intervals. Climate zones are defined based on mean annual precipitation (Pr): arid (Pr ≤ 200 mm/year), semi-arid/humid (200 <Pr ≤ 800 mm/year), and humid (Pr > 800 mm/year).

indicating a reduced cooling effect driven by declining water inputs. The largest daytime weakening trends occurred in arid regions (0.20 K or 9% per decade), while smaller or non-significant trends were found in semi-arid, semi-humid, and humid zones (Fig. 1f–h). In contrast, nighttime LST exhibited a consistent strengthening of cooling effects nationwide, most prominently in arid zones (−0.09 K per decade; Fig. 1j). This divergent day-night pattern was consistent across all climate regions and mirrored at the provincial scale (Supplementary Fig. 3), suggesting a fundamental shift in how irrigation influences land surface energy dynamics.

Temporal trends in IWU strongly correlated with changes in LST cooling. Nationally, reductions in IWU were tightly associated with weakened daytime cooling and enhanced nighttime cooling ($R^2 = 0.76$ and 0.78, respectively; Fig. 1m). Regionally, IWU trends were strongly correlated with daytime LST changes in arid and humid areas ($R^2 = 0.74$, 0.78, Fig. 1n, p). Similar relationships were found across provinces experiencing pronounced LST trends (Supplementary Fig. 3). Interestingly, in semi-arid and semi-humid regions, nighttime LST was more sensitive to IWU changes than daytime LST (Fig. 1o), suggesting the presence of additional drivers—such as vegetation dynamics or shifts in energy flux components—that may moderate daytime responses.

Spatial and seasonal patterns of land surface cooling trends

Spatially, 58% of irrigated grid cells (at 0.5° resolution) across China exhibited statistically significant daytime ΔLST trends over the 2001–2020 period (Fig. 2a). Among these, two-thirds showed a positive trend, meaning either a weakening of daytime cooling (in areas with initially negative ΔLST like Northwest China) or an intensification of surface warming (where ΔLST was already positive like South China, Supplementary Fig. 2c). At night, 46% of grid cells exhibited significant ΔLST trends, with 76% of these showing negative trends (Fig. 2b), signifying an intensification of nighttime cooling. This spatial dominance of enhanced nocturnal cooling was consistent across climate zones, with particularly strong signals emerging in inland drylands and northern irrigated provinces (Supplementary Fig. 3).

Seasonal trends further clarify how the impacts of WSI vary temporally and geographically. The reduction in daytime cooling was most pronounced during later summer and early spring in arid regions, especially in August when the average irrigation cooling effect reached -5.06 ± 0.39 K and weakened rapidly by 0.52 K per decade (Fig. 2c, Supplementary Fig. 2). This seasonality likely reflects the peak in evapotranspiration demand, coinciding with increased crop water stress and reduced soil evaporation under WSI systems. Conversely, the enhancement of nighttime cooling was strongest in late autumn to early spring, aligning with regional irrigation practices for soil moisture conservation and salt leaching during the non-growing season[29–31]. Under these cooler conditions and lower evaporative demand, the combination of reduced soil moisture and diminished thermal inertia likely amplified radiative cooling, contributing to more pronounced nocturnal temperature declines.

Water-saving irrigation reshapes surface energy partitioning

The adoption of WSI practices has fundamentally altered surface energy partitioning, especially by reshaping the balance between latent and sensible heat fluxes. Over the 2001–2020 period, irrigation increased latent heat flux (ΔLE) by 3.81 ± 0.21 W m^{-2} and reduced sensible heat flux (ΔHE) by -2.86 ± 0.26 W m^{-2} relative to non-irrigated conditions across China (Supplementary Text 2 and Supplementary Fig. 4). In contrast, changes in both outgoing longwave radiation and reflected shortwave radiation were minimal, indicating that irrigation-induced energy shifts primarily affected the turbulent heat flux components.

Long-term trends in these energy fluxes exhibit clear spatial divergence. The magnitude of both ΔLE and ΔHE increased markedly in northern China, particularly in arid regions, while declining or remaining stable in southern humid zones (Fig. 3a, b). Two-thirds of irrigated grid cells showed significant trends in ΔLE, with 57% experiencing a positive trajectory. The ΔLE trend reached 2.04 W m^{-2} per decade in arid zones (Fig. 3d), despite the concurrent reduction in IWU. This counterintuitive increase in ΔLE under water-saving conditions likely reflects sustained or enhanced crop transpiration driven by vegetation greening[32,33]. Advances in agricultural practices, such as improved crop varieties, no-till farming, and precision fertilization, have increased vegetation vigor and greenness over irrigated croplands[34,35]. This is supported by observed increases in EVI (Enhanced Vegetation Index) as well as evapotranspiration (Supplementary Fig. 5). Moreover, leveraging a high-resolution evapotranspiration dataset (PML_V2[36], Methods), we observe a consistent trend in rising transpiration and declining soil evaporation (Supplementary Fig. 6). These findings suggest that WSI shifts the source of evapotranspiration away from bare soil and toward plant transpiration, maintaining or even enhancing plant water use despite constrained irrigation inputs. In contrast, humid regions, where WSI uptake remains limited and traditional flood irrigation persists, exhibited significantly smaller ΔLE values and a declining trend of −0.11 W m^{-2} per decade (Fig. 3f; Supplementary Fig. 4a). This decrease may reflect a transition in cropping systems, such as the replacement of double-rice cultivation with single-season rice, thereby reducing vegetation greenness and annual evapotranspiration demand[34].

Trends in ΔHE also shows north-south differences (Fig. 3b). Nationwide, 45% of grid cells show significant declines in ΔHE, particularly in the North, resulting in an increasing magnitude (e.g., 3.05 W m^{-2} per decade in arid regions, Fig. 3d). At the provincial level, spatial patterns of energy flux trends mirrored those at grid scale (Supplementary Fig. 7), reinforcing the dominant role of northern irrigated croplands in reshaping surface energy balance under WSI expansion.

Rising Bowen ratio explains reduced daytime cooling

The observed attenuation of daytime irrigation cooling under water-saving practices is primarily driven by a shift in surface energy partitioning, as quantified by the Bowen ratio (the ratio of sensible to latent heat flux). A rising Bowen ratio indicates that a larger fraction of available energy is being converted into sensible heat—directly warming the air—rather than being dissipated as latent heat through evapotranspiration.

Over the past two decades, both the ratio of ΔHE to ΔLE and the absolute change in the Bowen ratio (Δ(HE/LE)) have shown consistent and significant intensification across China (Fig. 3k–r). Nationally, the Bowen ratio magnitude increased by approximately 0.13 per decade ($p < 0.05$), with particularly strong trends in arid regions. These trends reflect a persistent imbalance: change in ΔHE outpaced that in ΔLE, shifting the surface energy balance toward warming. This imbalance is critical in explaining the weakening of daytime cooling under WSI. Although vegetation greening (reflected in rising EVI) has sustained or even enhanced LE in some regions (Supplementary Fig. 5), the concurrent intensification of ΔHE has exerted a stronger warming influence. As a result, the net effect of irrigation under reduced water use has transitioned toward indirect daytime warming.

Quantitatively, the warming contribution from ΔHE exceeded the cooling contribution from ΔLE in most regions, particularly in areas with a large and rising Bowen ratio (e.g., −0.61 K vs. −0.40 K per decade in arid zones; Supplementary Fig. 8). This shift underscores a critical biophysical trade-off: even when total evapotranspiration is sustained through crop adaptation, the ability of irrigation to dissipate surface heat and cool the land is diminished under water-saving practices. Put simply, less water per unit area combined with higher sensible heat production leads to a diminished biophysical cooling capacity. Together, these findings provide a mechanistic explanation for the attenuated cooling effects of irrigation during the daytime: while plant-mediated processes partially offset the effects of reduced water inputs, the rising dominance of sensible heat flux results in a diminished cooling effect.

Attribution analysis: irrigation water use as the dominant driver

To disentangle the drivers of observed changes in irrigation-induced LST effects, we conducted a multi-factor attribution analysis incorporating IWU, background climate conditions (precipitation, solar radiation, air temperature, and wind speed), and vegetation greening (ΔEVI, the difference in EVI between irrigated and non-irrigated croplands). Results from multiple

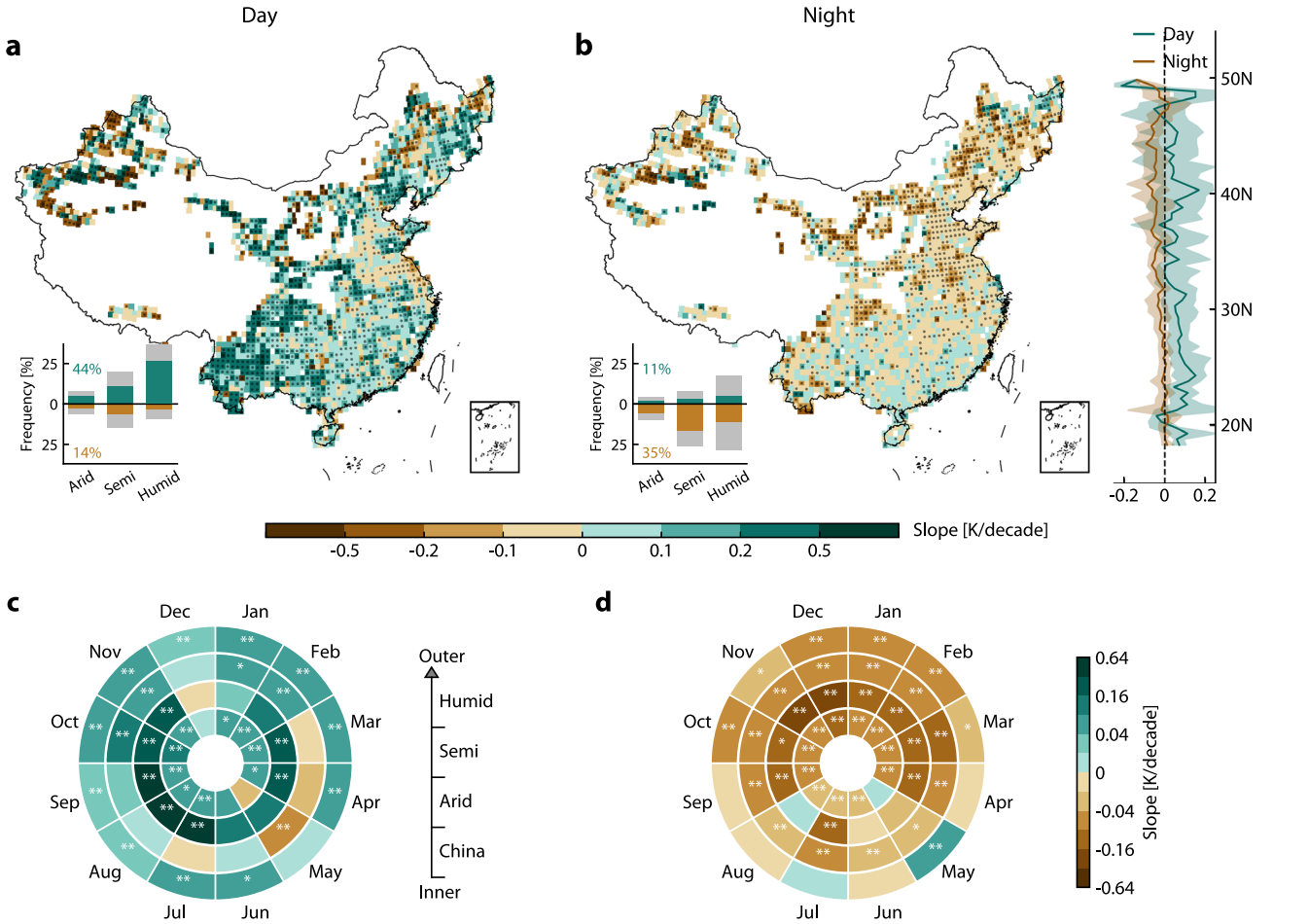

Fig. 2 | Spatial and seasonal patterns of trends in irrigation-induced land surface temperature change (ΔLST) from 2001 to 2020. a, **b** Spatial distribution of ΔLST trends at 0.5° resolution for daytime (**a**) and nighttime (**b**). Black dots indicate grid cells with a statistically significant trend ($p < 0.1$). Right-side panels show the latitudinal median (solid line) and interquartile range (shaded area: 25th–75th percentiles). Inset histograms show the frequency of grid cells with significantly positive (green), negative (brown), or non-significant (gray) trends ($p < 0.1$ and $p > 0.1$, respectively) across climate zones. "Semi" represents semi-arid and semi-humid regions. The numbers indicate the percentage of total grids with a significantly positive (green) and negative (brown) trend, respectively. **c**, **d** Seasonal trends in ΔLST for daytime (**c**) and nighttime (**d**), respectively. $^{**}p < 0.05$, $^{*}p < 0.1$ based on the Student's *t*-test.

linear regression models reveal that declining IWU—representing the widespread adoption of WSI—was the dominant driver of ΔLST trends across China. Nationally, IWU alone explained 77% of the variance in the daytime ΔLST trend and 87% of the nighttime trend (Fig. 4a, e). In arid zones, where irrigation plays a pivotal role in land-atmosphere interaction, the modeled IWU-driven ΔLST changes in the daytime (0.21 K per decade) and nighttime (−0.10 K per decade) closely matched the observed trends (Fig. 4b, f). This alignment strongly supports the hypothesis that reductions in irrigation intensity are the primary determinant of diurnal thermal changes in irrigated landscapes. In semi-arid and semi-humid regions, however, the IWU-driven daytime indirect warming was more muted and was partially offset by vegetation greening, leading to a non-significant net trend in ΔLST (Fig. 4c). Partial correlation analysis results (presented in Supplementary Text 3 and Supplementary Fig. 9) further confirm the leading role of IWU in regulating ΔLST across all climate zones.

To capture the spatial variability in driver importance, we also mapped the grid-scale contribution coefficients of IWU, ΔEVI, and climate variables across China (Supplementary Figs. 10, 11). These maps show the widespread dominance of IWU as the leading driver of LST trends, particularly in northern and western regions where WSI adoption has been most aggressive. Overall, this attribution analysis confirms that the reduction in IWU, though beneficial for conserving water resources, has altered the land surface energy balance in ways that reduce the climate buffering capacity of irrigation, especially during the daytime.

Causal pathways from irrigation water use to land surface temperature

To elucidate the causal relationships among IWU, vegetation greenness (ΔEVI), surface energy fluxes, and LST, we applied a structural equation modeling approach both at the national and climate-zone scales. We find that both IWU and ΔEVI significantly affect LST across China, albeit via different mechanisms and magnitudes (Fig. 5a). IWU exerts a strong positive influence on sensible heat flux (path coefficient = +0.76), indicating that reductions in IWU increase ΔHE and reduced cooling. In contrast, ΔEVI is negatively associated with ΔHE (−0.32), suggesting that crop greening suppresses sensible heat release, providing a localized cooling effect. Regarding latent heat, IWU exhibits a negative relationship with ΔLE (−0.57), while ΔEVI is positively associated with ΔLE (+0.50), reflecting that irrigation reductions limit total evapotranspiration, whereas vegetation vigor—linked to improved crop management—helps sustain transpiration.

Importantly, the path coefficient from ΔHE to LST (+4.65) was substantially larger in magnitude than that from ΔLE to LST (−3.32), suggesting that the warming effect of enhanced sensible heat outweighs the cooling effect of latent heat under reduced water availability. While improved vegetation conditions partly buffer against thermal stress through increased transpiration, this effect is insufficient to offset the dominant warming pathway mediated by ΔHE. Additionally, IWU exerts a minor influence on net shortwave radiation through changes in albedo, due to shifts in surface reflectivity as soils become drier and brighter. However, this

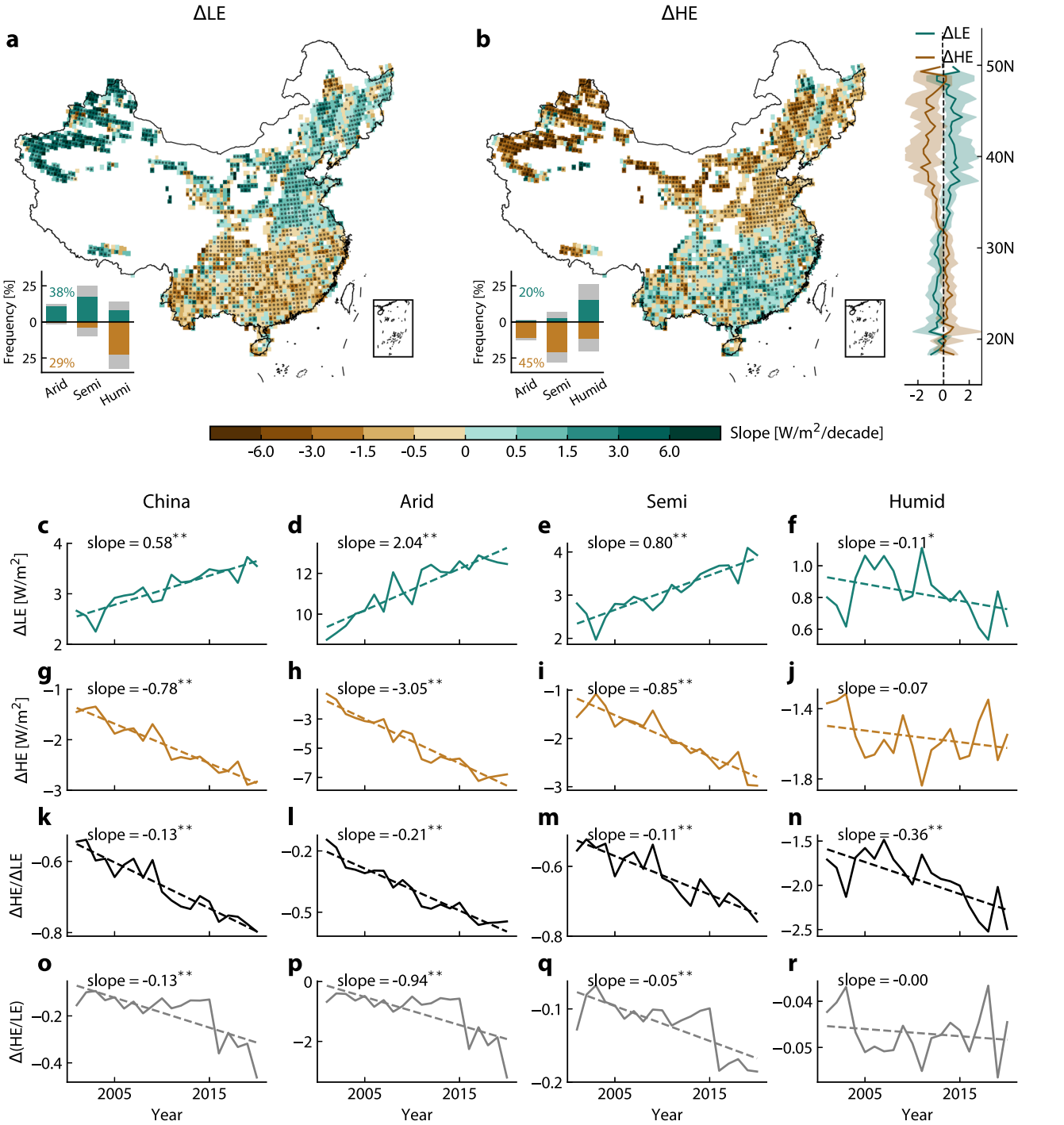

Fig. 3 | Trends in irrigation-induced surface energy flux changes from 2001 to 2020. a, **b** Spatial distribution of trends in latent heat flux (ΔLE; a) and sensible heat flux changes (ΔHE; b) due to irrigation at 0.5° grid resolution. Black dots indicate statistically significant trends ($p < 0.1$). Right-side panels show the latitudinal median (solid line) and interquartile range (shaded area). Inset histograms show the frequency of grid cells with significantly positive (green), negative (brown), or non-significant (gray) trends, following the same conventions as Fig. 2. **c**, **d** Trends in ΔLE across China (**c**), arid (**d**), semi-arid/semi-humid (**e**), and humid regions (**f**). **g**–**j** Trends in ΔHE. **k**–**n** Trends in ΔLE/ΔHE. **o**–**r** Trends in Δ(HE/LE). $^{**}p < 0.05$, $^{*}p < 0.10$ based on the Student's *t*-test.

radiative pathway plays a minimal role in the overall LST response. Notably, the strength of these influencing mechanisms varies spatially (Supplementary Fig. 12), for example, the largest path coefficient from IWU to LE appears in arid regions, while EVI to LE dominates in semi-arid and semi-humid regions. In contrast, the effect is negligible in humid areas. Together, these results underscore a robust causal chain from reduced IWU to reduced daytime cooling, driven primarily by increased sensible heat flux and only partially mitigated by vegetation greening. This mechanistic understanding reinforces earlier findings and emphasizes that while WSI promotes agricultural water savings, it alters the surface energy budget in a way that diminishes irrigation's climate mitigation capacity.

While daytime ΔLST changes under WSI are primarily governed by shifts in energy partitioning, the mechanisms underlying intensified nighttime cooling differ and are rooted in soil thermal properties and atmospheric radiative feedbacks. Generally, reduced IWU leads to lower soil moisture, which in turn decreases the soil volumetric heat capacity—its

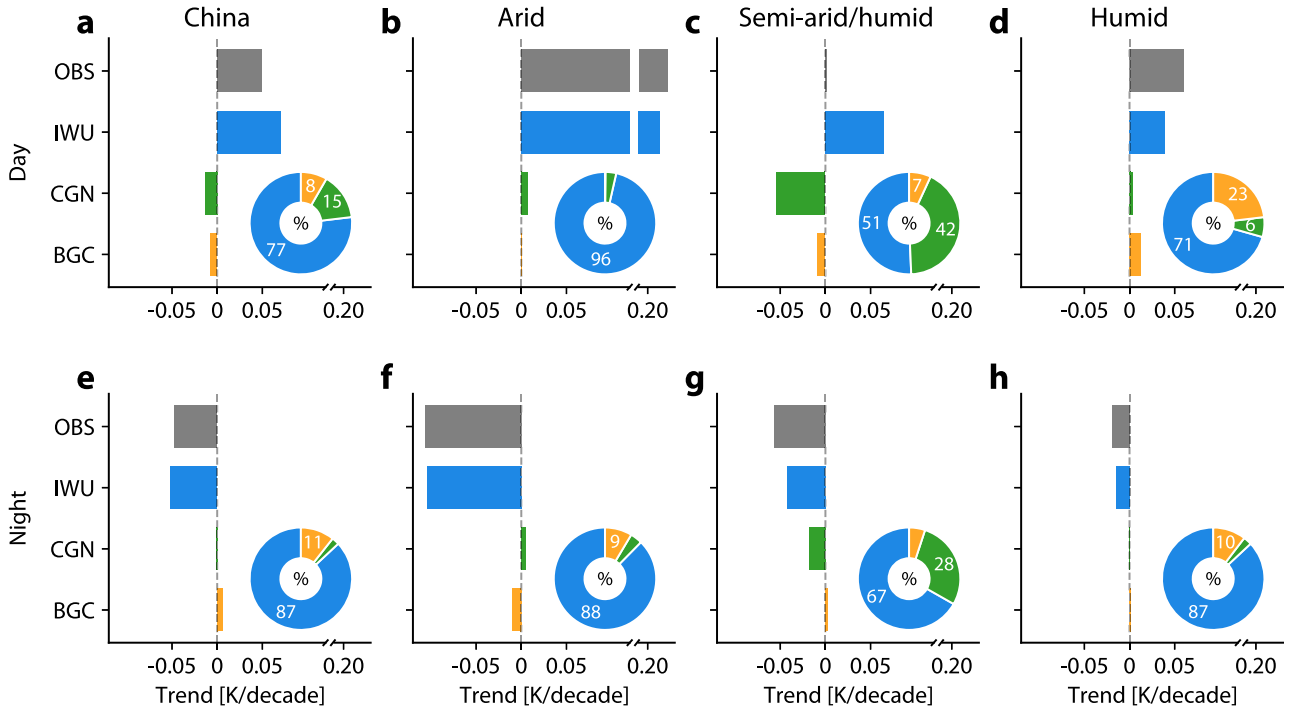

Fig. 4 | Drivers of observed ΔLST temporal trends. Mean contributions of irrigation water use (IWU), crop greening (CGN), and background climate (BGC) to observed trends (OBS) in irrigation-induced land surface temperature (ΔLST) trends in China (**a**), arid (**b**), semi-arid/humid (**c**), and humid (**d**) regions. **e–h** Same as **a–d** but for nighttime. Crop greening is characterized by the increase in enhanced vegetation index (ΔEVI). Background climate includes precipitation, air temperature, solar radiation, and wind speed. Inset pie charts depict the relative contribution of IWU, CGN, and BGC to the observed ΔLST trends (Methods, Eq. (10)).

ability to store and release thermal energy (Fig. 5b). Drier soils exhibit lower thermal inertia and cool more rapidly at night, amplifying nocturnal temperature drops[24]. This is corroborated by the strong positive partial correlation between IWU and nighttime ΔLST (Supplementary Fig. 9e–h). This thermal effect is further reinforced by changes in land-atmosphere radiative exchange. Under WSI, diminished soil heat content reduces upward ground heat flux and longwave radiation. Simultaneously, reduced evapotranspiration lowers near-surface humidity and cloud formation, weakening the greenhouse effect of atmospheric water vapor and decreasing downward longwave radiation from the atmosphere[37,38]. These compounding factors—lower soil heat storage, reduced surface humidity, and weaker atmospheric insulation—together enhance nighttime radiative cooling. These effects are particularly pronounced in arid and semi-arid regions, where baseline soil moisture is already low and the atmosphere is more sensitive to changes in land surface hydrology.

In sum, the above analyses and supporting evidence highlight that WSI alters both the turbulent and radiative components of the surface energy balance, generating a distinct diurnal signature: reduced daytime cooling but intensified nighttime cooling. These shifts in thermal dynamics may influence plant phenology[39], risk of frost, and land-atmosphere feedbacks, emphasizing the need to consider WSI not only in terms of water conservation but also its broader implications for local and regional climate regulation.

Discussion

This study provides the first large-scale observational evidence that widespread adoption of water-saving irrigation can weaken irrigation's biophysical climate benefits, most notably its daytime cooling effect. Over the past two decades, irrigation water use per hectare has declined significantly across China, coinciding with attenuated daytime land surface cooling and strengthened nighttime cooling. These contrasting diurnal responses, which are most pronounced in arid regions, stem from shifts in surface energy partitioning and thermal storage: increased sensible heat flux drives weakened daytime cooling, while reduced soil moisture and longwave insulation accelerate nighttime cooling. Although vegetation greening associated with improved crop management partly sustains transpiration and offsets warming[40], it cannot fully compensate for the loss of latent heat under lower water inputs. These findings reinforce the critical trade-off between improved water-use efficiency and the land surface's capacity to buffer climate warming. While our study centers on China, the insights are broadly applicable to other intensively irrigated regions undergoing similar transitions under mounting water stress.

Irrigation has long served as a cornerstone of agricultural resilience, especially in water-scarce regions, by securing yields and mitigating heat stress[1,2]. However, it also modifies land-atmosphere interactions by altering surface energy balances, local temperatures, and even regional precipitation patterns[7,8,11,41]. The expansion of WSI technologies, such as drip and sprinkler systems, now introduces a paradox in climate-smart agriculture: while these methods conserve water and sustain crop productivity, they may simultaneously reduce the cooling capacity of irrigated lands. In many regions, this shift from traditional to more efficient irrigation methods likely reduces the ability of irrigation to buffer climate warming[26]. Despite its growing relevance, this trade-off remains largely absent from current Earth system models and climate impact assessments[11,19]. Most models treat irrigation as a static, spatially uniform process, failing to account for changes in method, intensity, or seasonal dynamics[6,7,21]. Such simplifications risk overestimating irrigation's future cooling effect, especially under increasing water stress. Our findings underscore the urgent need for Earth system models to incorporate evolving irrigation strategies—including the magnitude and timing of water application, surface energy partitioning, and crop feedbacks—to improve climate projections, guide adaptation strategies, and inform policies that jointly advance agricultural resilience, resource efficiency, and thermal risk mitigation.

The climate impacts of WSI in China are spatially heterogeneous, with the most pronounced indirect warming occurring in arid zones. In arid regions, where agricultural production heavily relies on intensive irrigation, escalating water scarcity and cross-sectoral water competition have

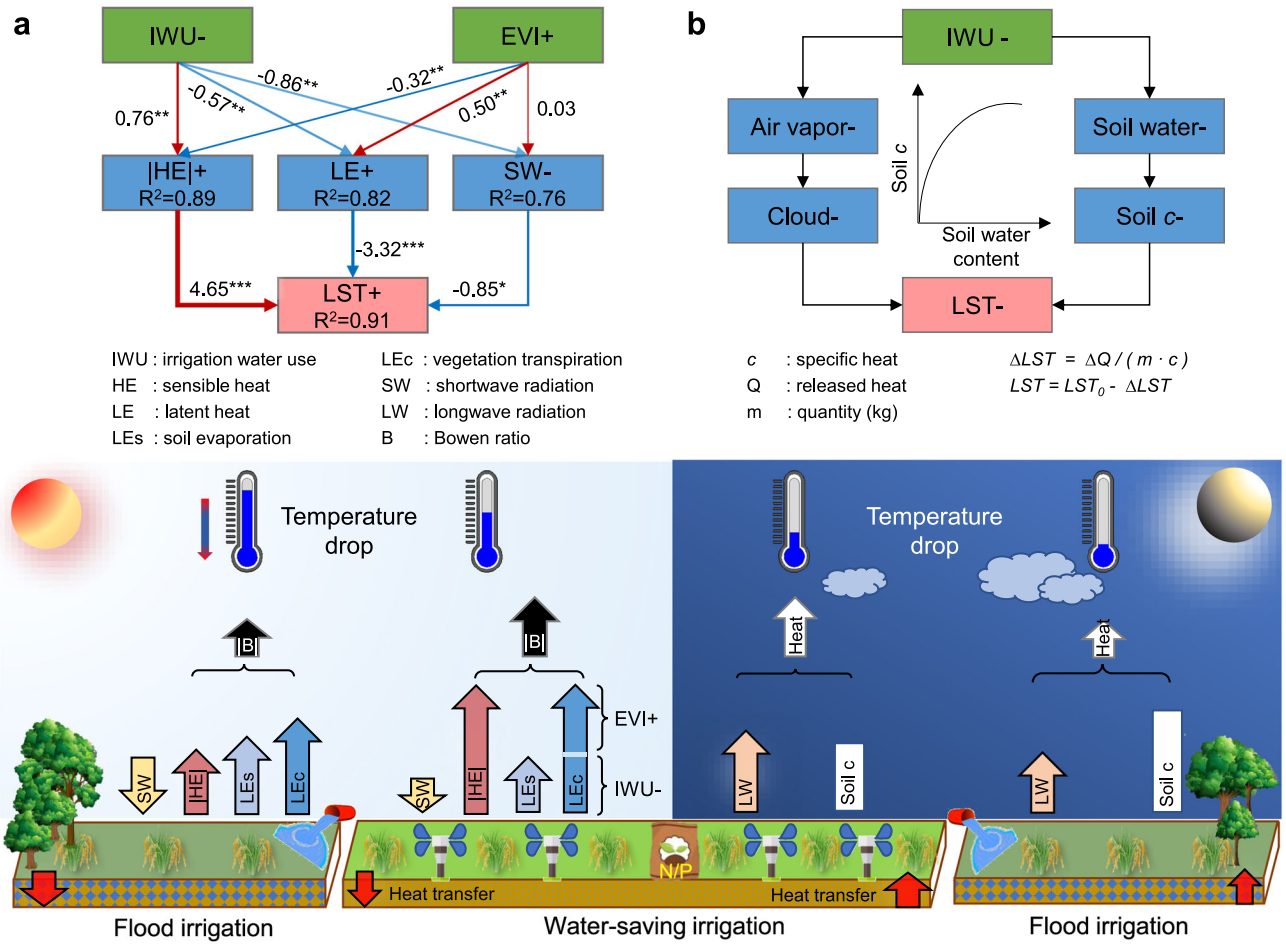

Fig. 5 | Mechanistic pathways of irrigation-induced temperature change under flood and water-saving irrigation regimes. a Daytime mechanisms. **b** Nighttime mechanisms. Panel (**a**) shows results from the national-scale structural equation model (SEM), quantifying the direct and indirect effects of irrigation water use (IWU) and vegetation greenness (ΔEVI) on land surface temperature (ΔLST) via energy fluxes. Path coefficients are standardized (**$p < 0.01$, *$p < 0.05$). Red and blue lines represent positive and negative effects, respectively. R^2 denotes model explanatory power. |HE| indicates the absolute magnitude of sensible heat flux, since HE change is negative by convention. Note that HE, LE, SW, and EVI represent the difference between irrigated and non-irrigated areas. The nighttime mechanism (**b**) is conceptually illustrated based on soil thermal dynamics and radiative feedbacks.

facilitated rapid WSI expansion, leading to significant attenuation of the biophysical cooling[16]. Taking Xinjiang as an example, WSI techniques were introduced in the late 1970s by the Xinjiang Production and Construction Corps and were gradually promoted to the whole of Xinjiang after 1998, leading to a 130% expansion of the WSI area and 26% reduction of IWU since the 21st century[42]. As a result, significantly weakened irrigation cooling effects on surface air temperature (an average increase of 0.30 °C in growing-season temperature) and LST (daytime weakening trend: 0.21 °C per decade) were observed in Xinjiang in the last two decades[22,23]. Specifically, the declining gaps of climatic factors (i.e., LST, ET, and VPD, etc.) between farms inside and outside Xinjiang Production and Construction Corps in our previous regional study[23] stand as a good corroboration of the attenuated irrigation cooling effect in arid regions due to increasing WSI. However, semi-arid and semi-humid regions—where the original irrigation cooling effect was not as evident as in arid regions (Supplementary Fig. 2a)—exhibited muted thermal trends. This minimal change is largely attributed to vegetation greening, which enhances transpiration and offsets the indirect warming trend (Fig. 4c and Supplementary Fig. 9c).

In contrast, the promotion of WSI appears to insensify the warming trend in humid regions, likely due to a weakened trend in vegetation greening within irrigated areas relative to non-irrigated areas (Supplementary Fig. 5d). This lag in greening, closely associated with reduced evaporative cooling (Supplementary Fig. 5l) may be linked to a decline in cropping intensity, such as the shift from double to single rice cultivation[34]. Meanwhile, the promotion of WSI has further reduced soil-driven evaporative cooling (Supplementary Fig. 6l), thereby exacerbating the warming effect. However, this impact is partially offset by a decrease in the absorbed solar radiation due to higher surface albedo from "brighter" soils (Supplementary Fig. 8l, Supplementary Fig. 10e).

The weakening of irrigation-induced cooling under WSI may have tangible consequences for food security and human thermal exposure. Many staple crops such as maize, wheat, and rice are highly sensitive to temperature extremes, particularly during reproductive stages, and even short-lived heatwaves can cause substantial yield losses[43]. The attenuation of daytime cooling in irrigated regions could reduce the protective buffer that irrigation has historically provided against heat stress, especially during critical growth periods[44]. In densely populated agricultural regions, this reduced cooling effect may also exacerbate human heat exposure, increase cooling energy demand, and undermine labor productivity during hot periods[45]. Studies suggest that WSI can lead to small but measurable increases in ambient temperature and vapor pressure deficit, potentially amplifying crop water demand even as total water use declines[22,26]. Nevertheless, the reduced water use associated with WSI may help alleviate moist heat stress[26]. Large-scale irrigation has been shown to increase humidity, which in turn raises the maximum wet bulb temperature—exacerbating deadly heat conditions and threatening the ability of local farmers to work outdoors[46,47]. These findings highlight the need to critically assess the resilience of agroecosystems and rural communities under climate-smart

irrigation strategies, emphasizing the importance of integrative planning that balances water conservation with thermal regulation and crop productivity.

Importantly, the observed nighttime cooling trends carry both potential benefits and risks. Enhanced nocturnal cooling may reduce plant respiration losses[39], limit nighttime heat stress in crops and humans[48], and potentially lower residential and industrial cooling energy demand in warm climates[49]. These effects could provide relief in heat-prone conditions, particularly during the growing season and summer months when thermal stress is highest. However, these benefits are not universally positive. In cooler seasons, intensified nighttime cooling may elevate the risk of frost events, threatening crop productivity during sensitive phenological stages such as flowering or early growth[50]. Additionally, greater nocturnal surface cooling can strengthen temperature inversions and suppress vertical mixing, potentially exacerbating air pollution episodes and degrading air quality in affected areas[51]. The interplay between lower surface humidity, reduced cloud cover, and weakened greenhouse insulation under WSI further complicates these dynamics[52]. Future research should evaluate not only the ecological and agronomic consequences of stronger nighttime cooling, but also its meteorological feedbacks and public health implications, particularly in rapidly irrigated and urbanizing landscapes. Understanding these multifaceted effects is essential for developing irrigation strategies that optimize both water use and climate adaptation outcomes.

Compared to existing modeling studies in the Indo-Gangetic Plain and North China Plain that heavily rely on accurately simulating IWU and soil moisture content[25,26], our satellite-based results directly capture the actual impact of irrigation on LST, avoiding uncertainties from model parameterizations and coarse spatial resolutions. The use of a finer-resolution, China-specific irrigation dataset[28] enabled a more comprehensive assessment of the irrigation cooling effect using more geographically sufficient samples, which was challenging for previous studies. The observed decline in cooling effects associated with the increasing WSI is consistent with recent findings. For example, a local study in Northwest China, based on meteorological station data, reported that large-scale adoption of WSI led to indirect warming and drying trends[22,24]. Similarly, field experiments argued that drip irrigation increases sensible heat and raises soil temperature compared to traditional irrigation[42], further corroborating our findings. Unlike earlier studies using in situ observations or small-scale control experiments, our study reveals, for the first time, a country-scale pattern of the WSI's impact on LST. Notably, our results also uncover contrasting diurnal trends in the irrigation-induced cooling effect, a dimension rarely addressed before. In contrast to our earlier study focused solely on Xinjiang, China[23], this study covers a broader geographic extent, capturing spatial variations in the evolving cooling effects across four climate zones. Moreover, it provides the first integrative analysis of the underlying mechanisms, such as shifts in surface energy partitioning driven by the competing influences of crop greening and reduced IWU. These insights are essential for improving climate model representation and informing policies aimed at mitigating climate warming.

Despite the robustness of our findings, several limitations warrant consideration. First, the irrigation maps used in this study, while independently validated, can not fully capture intra-seasonal variability or field-level irrigation practices such as rotation, deficit irrigation, or timing of water application. Moreover, the irrigation cooling trends assessed here are confined to persistently irrigated areas over the past two decades. As a result, they may represent a conservative estimate of the actual trend magnitude, since newly irrigated regions adopting water-saving technologies were not included. Second, while we use per-hectare IWU as a proxy for WSI intensity, this metric may not accurately reflect on-the-ground irrigation efficiency or system type, particularly in mixed-use or smallholder systems. Furthermore, using declining IWU per unit area as a proxy of the increasing WSI adoption may not always be appropriate at the pixel level, as a reduced mean IWU could also result from a constant total IWU spread over an expanding irrigation area within the same region. Third, the LST data, although widely used, are sensitive to cloud cover, view angle, and surface emissivity variations, which may introduce overestimation or underestimation of the trends, particularly in humid regions where persistent cloudiness reduces observation frequency. Fourth, while our attribution framework and structural equation modeling help elucidate potential causal pathways, they are based on observational correlations and cannot fully substitute for controlled field experiments or process-based modeling[36]. In addition, due to limited data availability—particularly at the national scale—we were unable to explicitly control for potential confounders such as crop type, field management practices, or regional policy interventions, all of which could influence surface energy dynamics and LST trends. Future research that integrates ground-based measurements, crop-specific biophysical modeling, and more detailed irrigation metadata will be essential for improving the attribution of irrigation-induced effects and strengthening the generalizability of our findings across diverse agroecological contexts.

Looking ahead, irrigated croplands are expected to expand by 70 million ha by 2050, with annual blue water consumption reaching 1800 cubic kilometers[53,54]. WSI is widely seen as a key strategy for sustainable agriculture, aiming to reduce water use without sacrificing crop yields. Beyond addressing the water scarcity problem, climate change mitigation is also a critical concern for future agricultural development. Our results show that widespread WSI adoption tends to attenuate irrigation-induced cooling and potentially intensify existing warming trends. While irrigated systems generally buffer against climate extremes better than rainfed ones[3], the reduced cooling effect under WSI may undermine this advantage since the rising temperature has been reported to negatively affect grain yields[55]. Therefore, more strategic planning is needed to balance water conservation goals with the preservation of irrigation's climate benefits. For instance, the development of WSI should be guided by regional water availability and climatic context——prioritizing water-scarce areas to maximize water savings, while complementing it with management practices in humid regions that sustain both water efficiency and local climate regulation. In addition, integrating real-time climate data, crop models, and remote sensing can enable adaptive irrigation scheduling that maintains adequate evaporative fluxes to sustain cooling during critical crop growth periods. Furthermore, policy frameworks and incentive programs should be carefully designed to balance water-use efficiency with the co-benefits of irrigation-induced cooling—ensuring that efficiency gains do not inadvertently increase vulnerability to heat stress during critical periods such as heatwaves. This requires setting context-specific thresholds for water use reduction and ensuring smallholders have access to the tools, technologies, and knowledge needed to balance efficiency with climate resilience. Collectively, these strategies are essential for aligning water-saving interventions with the broader goal of maintaining thermal regulation in agricultural systems under a changing climate.

Methods

Irrigation and land cover data

We used a 500-m annual time-series irrigation area dataset across China from 2000 to 2019 (IrriMap_CN)[28,56]. This dataset was generated using machine learning applied to MODIS surface reflectance and spectral indices on the Google Earth Engine platform, achieving a mean accuracy of 81%[51]. To match the MODIS LST resolution, we resampled IrriMap_CN to 1 km using nearest-neighbor interpolation. To reduce uncertainty and exclude changes in irrigated extent, only pixels that remained irrigated throughout the 20 years were retained. To validate the irrigation cooling estimates derived from IrriMap_CN, we also employed an independent irrigation dataset (IrriMap_Meier) for the period 1999–2012. IrriMap_Meier was developed using a multiple decision tree model and incorporating NDVI time series and agricultural suitability maps[57]. It has been widely used in regional irrigation studies[58–60].

We utilized the National Land Cover Dataset of China (NLCD-China) to identify cropland and grassland areas. NLCD-China is based on visual

interpretation of Landsat imagery and provides land cover maps every 5 years since the 1980s, with an overall accuracy of over 90%[61]. We used the 1-km version to match MODIS LST resolution. Stable cropland and grassland pixels were identified by overlaying five NLCD maps (2000–2020), and non-irrigated reference areas were derived by excluding the stable irrigated areas.

The statistical mean IWU per hectare was from China Water Resources Bulletin for 2003–2020, comprising the water use data for each province except Hong Kong, Macao, and Taiwan. To obtain the water use data in four climate zones, we first assigned the provincial IWU data to all 1-km irrigated cropland pixels within the province and then aggregated them to each climate zone according to their geographical locations (see Fig. 1a–d).

MODIS and PML_V2 Dataset

LST data for 2001–2020 was obtained from the MOD11A2 product (Terra platform), which provides 8-day composites at 1 km resolution. LST is retrieved using a split-window algorithm based on MODIS thermal infrared bands 31 and 32[62]. Both daytime (~10:30 a.m. local solar time) and nighttime (~10:30 p.m.) values were used. We retained only data labeled as "good quality" or "other quality" with emissivity error ≤0.02 and LST error ≤1 K to ensure accuracy[63]. Surface albedo was derived from the daily black-sky albedo of the MCD43A3 product[64]. We retained only pixels flagged as best (0), good (1), or mixed quality (2) to ensure data integrity. Black-sky albedo was chosen due to its strong correlation with other albedo definitions[63]. Broadband surface emissivity was calculated as the average of MODIS bands 31 and 32. Vegetation greenness was represented using the EVI from MOD13A2, which provides 16-day composites at 1-km resolution[65]. EVI improves sensitivity over dense vegetation compared to NDVI and reduces atmospheric and soil background influences, making it suitable for eco-climatic analyses[66]. The use of MODIS-based variables from a consistent satellite platform ensures co-located, synchronous, and spatially consistent observations, which are critical for robust inter-variable comparisons.

Evapotranspiration (ET) was derived from the Penman-Monteith–Leuning V2 (PML_V2) product[36], which integrates MODIS-derived vegetation and surface properties with GLDAS meteorological forcing data at 500-m resolution and 8-day intervals. The dataset performs well against eddy covariance observations from 95 global flux towers and compares favorably with other benchmark ET products. PML_V2 partitions ET into transpiration, soil evaporation, and canopy interception. For this study, we aggregated all components to the monthly and annual total ET. ET (mm/day) was converted to latent heat flux (W m^{-2}) using a factor of 28.36 W m^{-2} per mm/day[67]. We also used MODIS ET data (MOD16A2), which is based on the Penman-Monteith equation[68], to validate the capacity of PML_V2 ET in capturing the observed changes in irrigation practices.

Climate and topography data

Background climate variables, including surface air temperature, precipitation, wind speed, and downward surface shortwave radiation, were obtained from the TerraClimate dataset[69]. TerraClimate provides monthly, high-resolution (4 km) global climate and water balance data by merging CRU Ts4.0, WorldClim, and JRA-55 using climatically aided interpolation. This dataset has been extensively used in studies of climate variability, change impacts, and ecological assessments[70]. Downward longwave radiation fluxes were derived from the FLDAS dataset, which offers gridded meteorological data for drought and food security monitoring[71].

Topographic information was acquired from the Shuttle Radar Topography Mission (SRTM) Digital Elevation Model (DEM) at 1-km resolution[72]. DEM data were primarily used to filter valid pixels by constraining elevation differences between irrigated and non-irrigated reference areas during pairwise comparisons (shown in the next section). All raster data (Supplementary Table 1) were resampled to a common resolution of 1 km using nearest-neighbor interpolation to match the spatial resolution of MODIS LST data.

Estimation of irrigation-induced LST change using pairwise comparison

The irrigation effect on LST was quantified as the LST difference (ΔLST) between irrigated and nearby non-irrigated areas (i.e., cropland and grassland) using:

$$\Delta LST = LST_{irrigated} - LST_{non-irrigated} \quad (1)$$

This pairwise comparison method assumes that both irrigated and non-irrigated pixels within a defined spatial window share similar background climate conditions, thus minimizing confounding factors.

We implemented a flexible window-searching algorithm to extract the irrigation effect on LST[21]. For each irrigated pixel, we defined a square window of initial size $L_0 = 31$ km and identified non-irrigated reference pixels within this window. A valid comparison requires at least $N = 10$ reference pixels with elevation differences E ≤ 50 m relative to the central irrigated pixel. If the condition was not met, the window size was incrementally enlarged up to $L_{max} = 101$ km. ΔLST was then calculated as the temperature difference between the irrigated pixel and the mean of all valid reference pixels. Positive ΔLST indicates a warming effect, while negative values reflect a cooling effect due to irrigation. We tested alternative parameters (e.g., $L_0 = 21, 41$ km; $N = 10, 20, 25$; $E = 60, 80, 100$ m), which yielded consistent results (Supplementary Figs. 13, 14). Notably, 95.6% of valid samples were detected within the default 31-km window (Supplementary Fig. 15). Other biophysical variables (i.e., ET, albedo, sensible heat flux, etc.) changed by irrigation were derived using the same method and then aggregated to different spatial (0.5° grid, climate zone, and country) and temporal (annual and seasonal) scales for trend analyses.

Validation of the irrigation map for estimating cooling effects

To validate the robustness of the results (i.e., ΔLST and ΔET) based on the irrigation map (IrriMap_CN), we replicated the calculation of ΔLST and ΔET by replacing IrriMap_CN with IrriMap_Meier and examined their consistency. It is worth noting that IrriMap_Meier was produced using a different method and input variables from IrriMap_CN. As shown in Supplementary Fig. 16, both ΔLST and ΔET calculated using the two irrigation maps have a consistent pattern over China and three climate zones, despite some discrepancies in magnitude, demonstrating the robustness of IrriMap_CN as an input for estimating irrigation cooling effects.

Surface energy balance and irrigation-induced energy flux changes

The surface energy balance is expressed as:

$$SW_{in} - SW_{out} + LW_{in} - LW_{out} = LE + HE + G \quad (2)$$

where LE is the latent heat flux, HE is the sensible heat flux, and G is the ground heat flux. SW_{in} and LW_{in} are the downward shortwave and longwave radiative fluxes, acquired from TerraClimate[69] and FLDAS[71], respectively. SW_{out} is the reflected shortwave radiative flux that can be expressed as $SW_{out} = \alpha \times SW_{in}$. α indicates ground surface albedo. LW_{out} is upward longwave radiative flux emitted from the ground and can be calculated from the surface temperature (T) and broadband emissivity (ε) using the Stefan–Boltzmann law:

$$LW_{out} = \sigma \varepsilon T^4 \quad (3)$$

where σ is the Stefan–Boltzmann constant (5.67×10^{-8} W m^{-2} K^{-4}), ε is calculated from the average of MODIS bands 31 and 32.

The energy flux changes induced by irrigation can be expressed as:

$$\Delta SW_{in} - \Delta SW_{out} + \Delta LW_{in} - \Delta LW_{out} = \Delta LE + \Delta HE + \Delta G \quad (4)$$

Assumptions of $\Delta SW_{in} = 0$, ΔG=0, and $\Delta LW_{in} = 0$ were made here because they are negligible within a small extent[73]. Thus, after rewriting and

simplifying the above equations, the change in the sensible heat flux can be expressed as:

$$\Delta HE = -\Delta\alpha \cdot SW_{in} - \Delta LW_{out} - \Delta LE \quad (5)$$

Validation of latent heat flux estimation

While validation of the methodology against ground-based measurements of latent heat flux would be favorable, no sufficiently dense or representative ground-based monitoring networks currently exist. Measurement from the Flux tower is an ideal choice, but we would need a large and well-distributed number of paired sites with contrasting irrigation types yet similar climate backgrounds, which are not available. As an alternative, we proposed a diagnostic to evaluate the robustness of the PML_V2 latent heat flux, which could be a source of uncertainty, against another data-driven LE product (MOD16A2)[68,74], which is one of the most commonly used ET/LE products in related studies and has the same spatial resolution (500 m) as the PML_V2 product. We replicated the calculation of time-series ΔLE between irrigated and non-irrigated croplands from 2001 to 2020 using the MODIS LE data via the space-for-time method (Eq. (1)). We then compared the ΔLE derived from PML_V2 and MODIS and found strong and significant ($p < 0.01$) correlations (Supplementary Fig. 17). As a result, we concluded that the capacity of the PML_V2 LE product to capture the observed changes in irrigation practices is adequate for our methodology and scope.

Decomposition of the energy balance contributions to LST

To identify how biophysical processes contribute to LST changes, we decomposed the energy budget following previous studies[7,73,75,76]. Combining Eqs. (2) and (3), we rearranged the term as:

$$\sigma\varepsilon LST^4 = SW_{in} + LW_{in} - SW_{out} - LE - (HE + G) \quad (6)$$

Neglecting changes in downward radiation, emissivity, ground heat flux, and isolating for temperature[73,76], we obtained the following equation to represent the LST change due to irrigation,

$$\Delta LST = \frac{1}{4\sigma LST^3}(-\Delta SW_{out} - \Delta LE - \Delta HE) \quad (7)$$

This equation partitions LST changes into components driven by changes in albedo (SW_out), latent heat, and sensible heat. The estimated ΔLST closely matched the observed values (Supplementary Fig. 18), suggesting that the key energy flux changes induced by irrigation were well captured.

Attribution of drivers to ΔLST trends

To disentangle the drivers of ΔLST changes, we conducted both partial correlation and multiple linear regression analyses. Climate variables included precipitation (Pr), air temperature (Ta), solar radiation (Sr), and wind speed (Ws); anthropogenic drivers included irrigation water use (IWU) and vegetation greenness (ΔEVI). We modeled ΔLST as:

$$\Delta LST = b_0 + b_1 \cdot IWU + b_2 \cdot Pr + b_3 \cdot Ta + b_4 \cdot Sr + b_5 \cdot Ws + b_6 \cdot \Delta EVI \quad (8)$$

The model was applied to time series (2003–2020) at the national and climatic zone levels. Before regression, variance inflation factor (VIF) tests confirmed no multicollinearity (Supplementary Fig. 19).

To determine each driver's contribution to ΔLST trends, we computed:

$$Trend_{\Delta LST,i} = b_i \cdot Trend_i \quad (9)$$

$$Contribution_i = \frac{|Trend_{\Delta LST,i}|}{\sum_i |Trend_{\Delta LST,i}|} \quad (10)$$

Structural equation modeling of irrigation impacts

To further clarify causal pathways, we applied structural equation modeling (SEM) to assess the direct and indirect effects of IWU and ΔEVI on ΔLST via energy fluxes. SEM is a multivariate approach that estimates standardized path coefficients from observed covariance matrices[77]. SEM estimates path coefficients via maximum likelihood estimation, minimizing the difference between observed and model covariance matrices. Many studies have used SEM to determine the causal relationships between phenomena and to test the latent variables that may exist[78,79]. Annual time series data from 2003 to 2020 (ΔLST, IWU, ΔEVI, ΔLE, ΔHE, and ΔSW_out) were averaged at the national or climate-zone scale. SEM was used to quantify the strength and direction of links between variables and evaluate whether changes in crop greenness could counteract the thermal effects of reduced irrigation.

Data availability

The MODIS data are publicly available at https://e4ftl01.cr.usgs.gov/; the NLCD-China dataset is freely downloaded from https://www.resdc.cn; the irrigation dataset is publicly available at https://doi.org/10.6084/m9.figshare.20363115.v1; the PML_V2 dataset is acquired from https://code.earthengine.google.com/?asset=projects/pml_evapotranspiration/PML/OUTPUT/PML_V2_8day_v014; the TerraClimate dataset is acquired from https://doi.org/10.7923/G43J3B0R; SRTM data are publicly available at https://srtm.csi.cgiar.org. Irrigation water use data is from the China Water Resources Bulletin published at http://www.mwr.gov.cn.

Code availability

The codes to reproduce all main and Supplementary Figs. are written with Python 3.9. Scripts are available at https://github.com/Chao21/Watersaving_Irrigation_CN or from the corresponding authors upon reasonable request.

Received: 3 July 2025; Accepted: 12 November 2025;
Published online: 03 December 2025

References

1. Gebrechorkos, S. H. et al. Warming accelerates global drought severity. *Nature* **642**, 628–635 (2025).
2. Chiang, F., Mazdiyasni, O. & AghaKouchak, A. Evidence of anthropogenic impacts on global drought frequency, duration, and intensity. *Nat. Commun.* **12**, 2754 (2021).
3. Wang, X. et al. Global irrigation contribution to wheat and maize yield. *Nat. Commun.* **12**, 1235–1242 (2021).
4. Rosa, L. Adapting agriculture to climate change via sustainable irrigation: biophysical potentials and feedbacks. *Environ. Res. Lett.* **17**, 063008 (2022).
5. ACM Transactions on Internet of ThingsMcDermid, S. et al. Irrigation in the Earth system. *Nat. Rev. Earth Environ*. **4**, 435–453 (2023).
6. Thiery, W. et al. Warming of hot extremes alleviated by expanding irrigation. *Nat. Commun.* **11**, 290–296 (2020).
7. Thiery, W. et al. Present-day irrigation mitigates heat extremes. *J. Geophys. Res. Atmos.* **122**, 1403–1422 (2017).
8. Mueller, N. D. et al. Cooling of US Midwest summer temperature extremes from cropland intensification. *Nat. Clim. Change* **6**, 317–322 (2016).
9. Zhang, C. et al. Characterizing spatial, diurnal, and seasonal patterns of agricultural irrigation expansion-induced cooling in Northwest China from 2000 to 2020. *Agric. Meteorol.* **330**, 109304–109317 (2023).
10. Yao, Y. et al. Compounding future escalation of emissions- and irrigation-induced increases in humid-heat stress. *Nat. Commun.* **16**, 9326 (2025).
11. Yao, Y. et al. Impacts of irrigation expansion on moist-heat stress based on IRRMIP results. *Nat. Commun.* **16**, 1045 (2025).

12. Braun, T. & Schlenker, W. Cooling externality of large-scale irrigation. *National Bureau of Economic Research Working Paper Series* (2023).
13. Yue, Z. et al. Water-saving irrigated area expansion hardly enhances crop yield while saving water under climate scenarios in China. *Commun. Earth Environ.* **6**, 295 (2025).
14. Jägermeyr, J. et al. Water savings potentials of irrigation systems: global simulation of processes and linkages. *Hydrol. Earth Syst. Sci.* **19**, 3073–3091 (2015).
15. Huang, G. et al. Water-saving agriculture can deliver deep water cuts for China. *Resour. Conserv. Recycl.* **154**, 104578 (2020).
16. Zhou, F. et al. Deceleration of China's human water use and its key drivers. *Proc. Natl. Acad. Sci. USA* **117**, 7702–7711 (2020).
17. Ju, Q., Du, L., Liu, C. & Jiang, S. Water resource management for irrigated agriculture in China: Problems and prospects. *Irrig. Drain.* **72**, 854–863 (2023).
18. Leng, G., Leung, L. R. & Huang, M. Significant impacts of irrigation water sources and methods on modeling irrigation effects in the ACME Land Model. *J. Adv. Model. Earth Syst.* **9**, 1665–1683 (2017).
19. Yao, Y. et al. Implementation and evaluation of irrigation techniques in the community land model. *J. Adv. Model. Earth Syst.* **14**, e2022MS003074 (2022).
20. Yuan, T. et al. Effects of different irrigation methods on regional climate in North China Plain: A modeling study. *Agric. Meteorol.* **342**, 109728 (2023).
21. Chen, L. & Dirmeyer, P. A. Global observed and modelled impacts of irrigation on surface temperature. *Int. J. Climatol.* **39**, 2587–2600 (2019).
22. Fu, J. et al. Amplified warming induced by large-scale application of water-saving techniques. *Environ. Res. Lett.* **17**, 034018 (2022).
23. Zhang, C. et al. Attenuated cooling effects with increasing water-saving irrigation: satellite evidence from Xinjiang, China. *Agric. Meteorol.* **333**, 109397–109409 (2023).
24. Fu, J., Kang, S. & Zou, M. Impacts and biophysical mechanisms of agricultural water saving on land surface temperature in Northwest China. *Agric. Water Manag.* **319**, 109804 (2025).
25. Liu, G., Wang, W. & Shao, Q. Recent decline of irrigation-induced cooling effect over the north china plain in observations and model simulations. *Geophys. Res. Lett.* **50**, e2022GL101973 (2023).
26. Ambika, A. K. & Mishra, V. Improved water savings and reduction in moist heat stress caused by efficient irrigation. *Earth's Future* **10**, e2021EF002642 (2022).
27. Zhong, Z. et al. Reversed asymmetric warming of sub-diurnal temperature over land during recent decades. *Nat. Commun.* **14**, 7189 (2023).
28. Zhang, C., Dong, J. & Ge, Q. IrriMap_CN: annual irrigation maps across China in 2000–2019 based on satellite observations, environmental variables, and machine learning. *Remote Sens. Environ.* **280**, 113184–113197 (2022).
29. Han, S. & Yang, Z. Cooling effect of agricultural irrigation over Xinjiang, Northwest China from 1959 to 2006. *Environ. Res. Lett.* **8**, 024039 (2013).
30. Qian, X. et al. Deep learning-based near-real-time monitoring of autumn irrigation extent at sub-pixel scale in a large irrigation district. *Agric. Water Manag.* **284**, 108335 (2023).
31. Xiong, L. et al. Modeling agro-hydrological processes and analyzing water use in a super-large irrigation district (Hetao) of arid upper Yellow River basin. *J. Hydrol.* **603**, 127014 (2021).
32. Forzieri, G. et al. Increased control of vegetation on global terrestrial energy fluxes. *Nat. Clim. Change* **10**, 356–362 (2020).
33. Piao, S. et al. Characteristics, drivers and feedbacks of global greening. *Nat. Rev. Earth Environ.* **1**, 14–27 (2020).
34. Zhang, G. et al. Spatiotemporal patterns of paddy rice croplands in China and India from 2000 to 2015. *Sci. Total Environ.* **579**, 82–92 (2017).
35. Qiu, B. et al. National-scale 10-m maps of cropland use intensity in China during 2018–2023. *Sci. Data* **11**, 691 (2024).
36. Zhang, Y. et al. Coupled estimation of 500 m and 8-day resolution global evapotranspiration and gross primary production in 2002–2017. *Remote Sens. Environ.* **222**, 165–182 (2019).
37. Li, H., Lo, M.-H., Ryu, D., Peel, M. & Zhang, Y. Possible increase of air temperature by irrigation. *Geophys. Res. Lett.* **49**, e2022GL100427 (2022).
38. Zhou, L., Dickinson, R. E., Tian, Y., Vose, R. S. & Dai, Y. Impact of vegetation removal and soil aridation on diurnal temperature range in a semiarid region: application to the Sahel. *Proc. Natl. Acad. Sci. USA* **104**, 17937–17942 (2007).
39. Peng, S. et al. Asymmetric effects of daytime and night-time warming on Northern Hemisphere vegetation. *Nature* **501**, 88–92 (2013).
40. Yu, L. et al. Asymmetric daytime and nighttime surface temperature feedback induced by crop greening across Northeast China. *Agric. Meteorol.* **325**, 109136–109145 (2022).
41. Greve, P. et al. Observational evidence of increased afternoon rainfall downwind of irrigated areas. *Nat. Commun.* **16**, 3415 (2025).
42. Yang, D. et al. Drip irrigation improves spring wheat water productivity by reducing leaf area while increasing yield. *Eur. J. Agron.* **143**, 126710 (2023).
43. Lesk, C. et al. Compound heat and moisture extreme impacts on global crop yields under climate change. *Nat. Rev. Earth Environ.* **3**, 872–889 (2022).
44. Li, Y. et al. Quantifying irrigation cooling benefits to maize yield in the US Midwest. *Glob. Change Biol.* **26**, 3065–3078 (2020).
45. Parajuli, S. P. et al. Impact of irrigation on farmworkers' heat stress in California differs by season and during the day and night. *Commun. Earth Environ.* **5**, 787 (2024).
46. Mishra, V. et al. Moist heat stress extremes in India enhanced by irrigation. *Nat. Geosci.* **13**, 722–728 (2020).
47. Kang, S. & Eltahir, E. A. B. North China plain threatened by deadly heatwaves due to climate change and irrigation. *Nat. Commun.* **9**, 2894–2902 (2018).
48. Wang, S. et al. Dual impact of global urban overheating on mortality. *Nat. Clim. Change* 15, 497–504 (2025).
49. Li, X. C., Zhao, L., Qin, Y., Oleson, K. & Zhang, Y. Elevated urban energy risks due to climate-driven biophysical feedbacks. *Nat. Clim. Change* **14**, 1056–1063 (2024).
50. Lamichhane, J. R. Rising risks of late-spring frosts in a changing climate. *Nat. Clim. Change* **11**, 554–555 (2021).
51. Niedźwiedź, T., Łupikasza, Małarzewski, E. B. & Budzik, T. Surface-based nocturnal air temperature inversions in southern Poland and their influence on PM10 and PM2.5 concentrations in Upper Silesia. *Theor. Appl. Climatol.* **146**, 897–919 (2021).
52. Hu, J. et al. Nocturnal surface radiation cooling modulated by cloud cover change reinforces PM2.5 accumulation: observational study of heavy air pollution in the Sichuan Basin, Southwest China. *Sci. Total Environ.* **794**, 148624 (2021).
53. Puy, A., Lo Piano, S. & Saltelli, A. Current models underestimate future irrigated areas. *Geophys. Res. Lett*. **47**, e2020GL087360 (2020).
54. Huang, Z. et al. Global agricultural green and blue water consumption under future climate and land use changes. *J. Hydrol.* **574**, 242–256 (2019).
55. Zhu, P. et al. Warming reduces global agricultural production by decreasing cropping frequency and yields. *Nat. Clim. Change* **12**, 1016–1023 (2022).
56. Zhang, C., Dong, J. & Ge, Q. IrriMap_CN: improved annual irrigation maps across China in 2000–2019 based on satellite imagery and machine-learning method. *figshare* **280**, 113184 (2022).

57. Meier, J., Zabel, F. & Mauser, W. A global approach to estimate irrigated areas—a comparison between different data and statistics. *Hydrol. Earth Syst. Sci.* **22**, 1119–1133 (2018).
58. Wine, M. L. Under non-stationarity securitization contributes to uncertainty and Tragedy of the Commons. *J. Hydrol.* **568**, 716–721 (2019).
59. Zhang, Z., Lin, A., Zhao, L. & Zhao, B. Attribution of local land surface temperature variations response to irrigation over the North China Plain. *Sci. Total Environ.* **826**, 154104–154155 (2022).
60. Yang, Q., Huang, X. & Tang, Q. Irrigation cooling effect on land surface temperature across China based on satellite observations. *Sci. Total Environ.* **705**, 135984–135993 (2020).
61. Liu, J. et al. Spatiotemporal characteristics, patterns, and causes of land-use changes in China since the late 1980s. *J. Geog. Sci.* **24**, 195–210 (2014).
62. Wan, Z. New refinements and validation of the MODIS land-surface temperature/emissivity products. *Remote Sens. Environ.* **112**, 59–74 (2008).
63. Li, Y. et al. Local cooling and warming effects of forests based on satellite observations. *Nat. Commun.* **6**, 6603–6610 (2015).
64. Schaaf, C. B. et al. First operational BRDF, albedo nadir reflectance products from MODIS. *Remote Sens. Environ.* **83**, 135–148 (2002).
65. Huete, A. et al. Overview of the radiometric and biophysical performance of the MODIS vegetation indices. *Remote Sens. Environ.* **83**, 195–213 (2002).
66. Liu, Z. et al. Surface warming in global cities is substantially more rapid than in rural background areas. *Commun. Earth Environ.* **3**, 219 (2022).
67. Abera, T. A., Heiskanen, J., Pellikka, P., Rautiainen, M. & Maeda, E. E. Clarifying the role of radiative mechanisms in the spatio-temporal changes of land surface temperature across the Horn of Africa. *Remote Sens. Environ.* **221**, 210–224 (2019).
68. Mu, Q., Zhao, M. & Running, S. W. Improvements to a MODIS global terrestrial evapotranspiration algorithm. *Remote Sens. Environ.* **115**, 1781–1800 (2011).
69. Abatzoglou, J. T., Dobrowski, S. Z., Parks, S. A. & Hegewisch, K. C. TerraClimate, a high-resolution global dataset of monthly climate and climatic water balance from 1958-2015. *Sci. Data* **5**, 170191–170202 (2018).
70. Kitzberger, T. et al. Projections of fire probability and ecosystem vulnerability under 21st century climate across a trans-Andean productivity gradient in Patagonia. *Sci. Total Environ.* **839**, 156303–156315 (2022).
71. McNally, A. et al. A land data assimilation system for sub-Saharan Africa food and water security applications. *Sci. Data* **4**, 170012–170030 (2017).
72. Jarvis, A., H.I. Reuter, A. Nelson, E. Guevara. Hole-filled SRTM for the globe: version 4: data grid, available from the CGIAR-CSI SRTM 90m Database: http://srtm.csi.cgiar.org (2008).
73. Duveiller, G., Hooker, J. & Cescatti, A. The mark of vegetation change on Earth's surface energy balance. *Nat. Commun.* **9**, 679–690 (2018).
74. Running, S., Mu, Q., Zhao, M. & Moreno, A. MODIS/Terra Net Evapotranspiration Gap-Filled Yearly L4 Global 500m SIN Grid V061. NASA EOSDIS Land Processes DAAC. https://doi.org/10.5067/MODIS/MOD16A3GF.061 (2021).
75. Luyssaert, S. et al. Land management and land-cover change have impacts of similar magnitude on surface temperature. *Nat. Clim. Change* **4**, 389–393 (2014).
76. Hirsch, A. L. et al. Modelled biophysical impacts of conservation agriculture on local climates. *Glob. Change Biol.* **24**, 4758–4774 (2018).
77. Grace, J. B., Anderson, T. M., Olff, H. & Scheiner, S. M. On the specification of structural equation models for ecological systems. *Ecol. Monogr.* **80**, 67–87 (2010).
78. Dong, L., Wu, C., Wang, X. & Zhao, N. Satellite observed delaying effects of increased winds on spring green-up dates. *Remote Sens. Environ.* **284**, 113363–113376 (2023).
79. Gao, S. et al. An earlier start of the thermal growing season enhances tree growth in cold humid areas but not in dry areas. *Nat. Ecol. Evol.* **6**, 397–404 (2022).

Acknowledgements

This study was supported by the Strategic Priority Research Program (Grant Nos. XDA23100400, XDA28060100), the CAS Youth Interdisciplinary Team Project (Grant No. JCTD-2021-04) of the Chinese Academy of Sciences and the National Natural Science Foundation of China (Grant Nos. 41871349, 42271375). X.X. was supported by the US National Science Foundation (Grant Nos. 1911955, 1946093).

Author contributions

Q.G., J.D. and C.Z. designed the study. C.Z. and J.D. performed the data analysis and wrote the paper with inputs from all co-authors. Q.G., W.T., Y.L., S.P., G.L., G.Z., Z.J., W.L., K.Z., X.Z., S.H. and G.Z. contributed to the interpretation of the results. W.T., Z.J. and X.X. helped to edit and improve the manuscript.

Competing interests

The authors declare no competing interests.

Additional information

Supplementary information The online version contains supplementary material available at https://doi.org/10.1038/s43247-025-03030-5.

Correspondence and requests for materials should be addressed to Quansheng Ge or Jinwei Dong.

Peer review information *Communications Earth and Environment* thanks George Paul and the other, anonymous, reviewer(s) for their contribution to the peer review of this work. Primary Handling Editors: Srinivas Rallapalli and Nandita Basu. [A peer review file is available].

[1]Institute of Geographic Sciences and Natural Resources Research, Chinese Academy of Sciences, Beijing, China. [2]University of Chinese Academy of Sciences, Beijing, China. [3]Department of Hydrology and Hydraulic Engineering, Vrije Universiteit Brussel, Brussels, Belgium. [4]State Key Laboratory of Earth Surface Processes and Resources Ecology, Beijing Normal University, Beijing, China. [5]Sino-French Institute for Earth System Science, College of Urban and Environmental Sciences, Peking University, Beijing, China. [6]Hubei Key Laboratory of Regional Ecology and Environmental Change, School of Geography and Information Engineering, China University of Geosciences, Wuhan, China. [7]Institute of Ecology, College of Urban and Environmental Science, Peking University, Beijing, China. [8]Department of Earth System Science, Ministry of Education Key Laboratory for Earth System Modeling, Institute for Global Change Studies, Tsinghua University, Beijing, China. [9]School of Geospatial Engineering and Science, Sun Yat-Sen University, Zhuhai, China. [10]State Key Laboratory of Simulation and Regulation of Water Cycle in River Basin, China Institute of Water Resources and Hydropower Research, Beijing, China. [11]College of Land Science and Technology, China Agricultural University, Beijing, China. [12]Department of Microbiology and Plant Biology, University of Oklahoma, Norman, OK, USA. ✉e-mail: geqs@igsnrr.ac.cn; dongjw@igsnrr.ac.cn